American Journal of Materials Science 2017, 7(6): 240-249
DOI: 10.5923/j.materials.20170706.03

Optical Characterization of Sn_xSe_y: SnO_2-Ni Prepared by Spray Pyrolysis for Photovoltaic Application

Nelson Mugambi[1,*], Mathew Munji[1], Robinson Musembi[2], John Gitonga[1], Geoffrey Gitonga[1]

[1]Department of Physics, Kenyatta University, Nairobi, Kenya
[2]Department of Physics, University of Nairobi, Nairobi, Kenya

Abstract Nickel doped tin oxide and tin monoselenide thin films were coated using spray pyrolysis on glass substrate at 375℃. Nickel doped tin oxide Precursor solution was prepared using Tin (II) Chloride ($SnCl_4.2H_2O$) and uniform concentration of ($NiCl_2.6H_2O$) of 0-10%. Precursor solution of tin selenide was prepared using alcoholic solution consisting of tin chloride ($Sncl_2.2H_2O$) and 1, 1-dimethl-2-selenourea ($C_3H_8N_2Se$). Samples of (Sn_xSe_y) were made in ratios of 1:0.4 to 1:1.4. The samples of tin selenide and Nickel doped tin oxide were characterized by measuring their optical properties using UV-VIS-NIR spectrophotometer 3700 DUV. The optical band gap of deposited tin selenide ranged between 1.39-2.23ev. The sample of $Sn:Se_{1.0}$ had the highest absorbance of over 46.26% and lowest transmittance of about 44.3% in the VIS-NIR region. The optical band gap of deposited Nickel doped tin oxide ranged between 3.65-3.75ev. The sample of Nickel doped tin oxide of 2% concentration had the highest transmittance of 86.2% and lowest absorbance of about 5.05% in the VIS-NIR region. These properties are suitable for window and absorber layers for application in photovoltaic cell. A conversion coefficient (η) of 0.4609% was obtained for Tin selenide (Sn_xSe_y) and nickel doped tin oxide (SnO_2: Ni) Solar cell.

Keywords Spray Pyrolysis, Tin oxide, Ni-doping, Selenide, Deposition temperature

1. Introduction

Energy is the main driver in any economy, because advancement in technology is directly or indirectly related to energy. Consumption of energy has steadily raised with sophistication of the world. Presently, growing concern is in venture of Photovoltaic cells which are inexpensive rather than major energy sources (fossil fuels) whose cost is ever increasing. Increase in petroleum prices have been contributed by the increase in demand due to human population causing upward pressure [19, 12].

The Silicon-based solar cell is principally used in photovoltaic industry. Silicon as an absorber material is limited because of its indirect band gap as compared to direct band gap materials [5]. The main advantage of thin film solar cells in comparison to silicon solar cells is that less energy is needed for processing, comparatively lower costs of the materials needed thus large scale production [30, 16].

SnSe is a group IV-VI semiconductor thin film having a wide range of applications due to its high absorption and suitability for optoelectronic applications because it has a narrow direct band gap energy which is around 1.1eV [6, 2, 15, 9, 10, 11, 14]. $SnSe_2$ thin films were obtained in the substrate temperature range from 270℃ to 300℃. At 270℃ $SnSe_2$ forms acceptable values of resistivity and mobility. The result obtained indicates the possibility to use these materials in a photovoltaic structure built completely by Ultra sonic Spray Pyrolysis technique [7, 18].

SnO_2 in its pure form has a wide band of approximately 3.7 eV and therefore a better n type semiconductor [27]. Pure SnO_2 film is inferior electrical conductor that is exceedingly transparent in the visible light. However their poor electrical conductivity can be improved by doping with impurities or controlling the stoichiometry [24, 29].

Doping tin dioxide by Fe, Co, Ni, and Cu (0–16 at %) has revealed that the dopants promote both the change of the film morphology and the decrease of grain size on the conducted research during the spray pyrolysis deposition. The doping influence on both the film morphology and the grain size is weakened at higher pyrolysis temperatures 450℃ [8]. SnO_2 doped with Nickel powder samples with dopant concentrations in the range of 3 at % to 15 at % were prepared using solid-state reaction. A decrease in optical band gap was revealed with the rise of Ni doping levels [13, 22, 28].

When light is illuminated on a semiconductor, intensity of transmission, absorption and reflection can be measured. A lot of information such as band gap of the material can be

* Corresponding author:
nelmug2013@gmail.com (Nelson Mugambi)
Published online at http://journal.sapub.org/materials

obtained pertaining a semiconductor from these optical effects [21]. Optical radiation is absorbed by excitation from one energy level to a higher energy level in semiconductors on condition that energy of radiation $h\upsilon$ is same to or more than the distinct in energy between the two participating levels. Transmittance through the film of thickness (d) and the intensity of radiation *I* dependence is of the form:

$$I = I_o \exp(-\alpha d) \quad (1)$$

where α is the absorption coefficient and I_0 is the initial intensity of radiation.

The reflection coefficient R and transmission coefficient T are the two vital quantities mostly measured and for normal incidence they are expressed as:

$$T = \frac{(1-R^2)\exp(-4\pi x/\lambda)}{1-R^2\exp(-8\pi x/\lambda)} \quad (2)$$

$$T = \frac{(1-n)^2+k^2}{(1+n)^2+k^2} \quad (3)$$

where, *x*, is the thickness of the sample, λ, is the wave length of radiation, *k*, extinction coefficient and *n*, the refractive index of the film. The reflectance R, and transmission T, of the system vary with optical constants, the thickness, *d*, of the film, refractive index *n*, extinction coefficient *k*, and the substrate of the index of refraction, n_s and the wavelength of light, λ [3].

The values of extinction coefficient *k*, film thickness *d*, and refractive index *n*, can be obtained by constructing enclose functions T_{max} and T_{min} from transmission measurements treated as continuous functions of wavelength λ. However:

$$n\left[N + (N^2 - n_s^2)^{\frac{1}{2}}\right]^{\frac{1}{2}} \quad (4)$$

where

$$N = \frac{(1+n_s^2)T_{max}\,T_{min}}{2+2n_s(T_{max}-T_{min})} \quad (5)$$

The two maxima or two minima can be used to calculate the thickness *d*, of the film using the expression:

$$d = \frac{M\lambda_1\lambda_2}{2[n(\lambda_1)\lambda_2 - n(\lambda_2)]\lambda_2} \quad (6)$$

where two extremes afoot at λ_1 and λ_2, gives the number of oscillations M.

Optical absorbance against wavelength gives the data which facilitates derivation of the transmission types and band gap energy by mathematical relationship shown below about the absorption edge.

$$\alpha = \frac{(h\upsilon - E_g)^{\frac{\beta}{2}}}{h\upsilon} \quad (7)$$

where h is the Planck's constant, υ is the frequency, whereas β takes the value of probable 1 or 4. β gives the transition kind whichever can be direct transition or indirect transition between the semiconductor states. For instance when β = 1, $(\alpha h\upsilon)^2$ against the photon energy ($h\upsilon$) is plotted, and the linear graph which cuts the photon energy ($h\upsilon$) axis gives the direct band gap value [30].

Scout software 32 bit software for windows 98/NT/2000/XP/Vista was used for the analysis and simulations of optical spectra such as absorbance, Attenuated total reflection (ATR), reflectance, transmittance, ellipsomery, and electroluminescence [25].

In this report we present reflectance, absorbance and transmittance measurements of SnSe and Nickel doped Tin Oxide on glass substrates prepared by spray pyrolysis and fabrication of p-n junction solar cell with glass/SnO_2: Ni/SnSe/Al.

2. Experimental

2.1. Sample Preparation and Deposition

Precursor solution was prepared using a 0.05M Tin (II) Chloride ($SnCl_4.2H_2O$) mixed with 0.05 M Nickel chloride 6-hydrate ($NiCl_2.6H_2O$) in distilled water and ethanol in the ratio 1:1 to get equal proportions. The solution was left for a week for complete dissolution.

Molar masses were used to calculate the percentage of dopant in SnO_2: Ni solution. Spray pyrolysis deposition conditions for the films were; substrate temperature of 375℃, rate of flow 6ml/min, air carrier gas of pressure 4.5×10^5 Pa, Nozzle-Substrate height of 20cm.

Tin monoselenide was prepared using precursor compounds which include 0.05M 1, 1-dimethyl-2-selenourea ($C_3H_8N_2Se$) compounds and 0.05M $SnCl_2.2H_2O$ mixed with distilled water and isopropyl alcohol in a ratio of 1:3. Molar masses were used to calculate the ratios of Sn_xSe_y. The ratios were 0.4, 0.6, 0.8, 1.0, 1.2, and 1.4. Thin films with different ratios of Selenium were fabricated on a microscope glass substrate. The deposition conditions for the films were; substrate temperature of 375℃, solution flow rate of 8ml/min, argon carrier gas of pressure 4.5×10^5 Pa, Nozzle-Substrate height of 20cm.

Deposition of the thin films was done using the spray pyrolysis technique as shown in figure 1. To produce SnO_2, Ni: SnO_2, Sn_xSe_y and Sn_xSe_y: Ni-SnO_2 films, the solution was sprayed onto a pre-heated normal microscope glass substrate using compressed air for the atomization of the precursor. At the heated surface, different types of ions in thermal motion are attracted or repelled under the action of electric forces. The more stable chemical composites are crystallized on the substrate forming a thin layer.

The solar cell device was fabricated in steps outlined below.

The n-type layer of transparent conducting SnO_2: Ni film was deposited first on to a glass substrate at a temperature of 648K and pressure of 4.5×10^5 Pa by Spray Pyrolysis technique.

A p-type layer of SnSe was deposited on to SnO_2: Ni on the same substrate at the same temperature and pressure of 4.41 x 10^5 Pa by Spray Pyrolysis technique.

Fabrication was completed by depositing Aluminium back contact of area $1cm^2$ on SnSe film. The thin film

obtained was SnSe - SnO_2: Ni which formed the p-n as shown in figure 2.

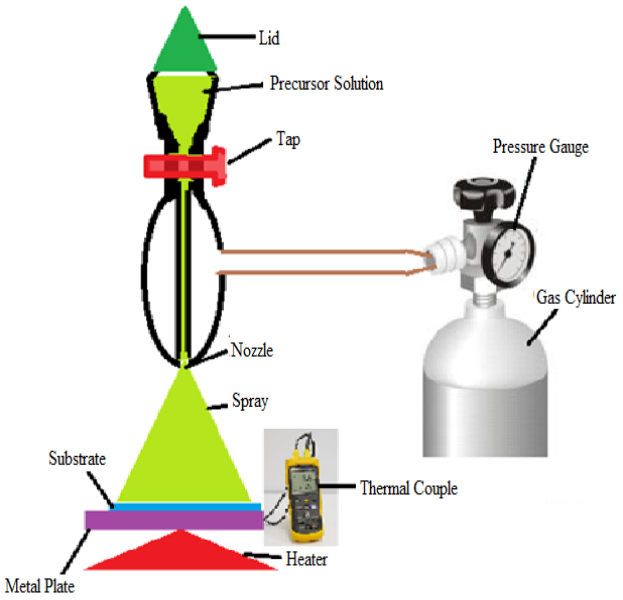

Figure 1. Spray Pyrolysis Setup

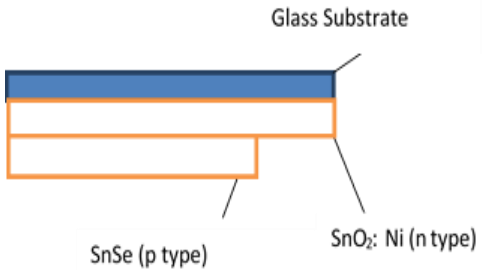

Figure 2. Schematic diagram of SnSe-SnO_2: Ni p-n Junction

3. Results and Discussion

3700 DUV UV-VIS-NIR Spectrophotometer was used to obtain the experimental data for transmittance and reflectance using the software of UV probe. Microsoft excel converted the data in its format from which spectra graphs were plotted separately for both tin selenide and Nickel doped Tin Oxide thin films using Microcal Origin 8.

3.1. Tin-Selenide (Sn_xSe_y)

3.1.1. Transmittance Spectra of Tin Selenide (Sn_xSe_y) Thin Films

The transmittance spectra for Sn_xSe_y samples at different Tin to Selenium ratios is shown on Figure 3. The graphs shows that transmittance were below 65% in the visible range (400nm-780nm). As wavelength of incident photon increases, it was observed that transmittance also increased. This was due to low absorption as a result of energy of photons being lower than the band gap.

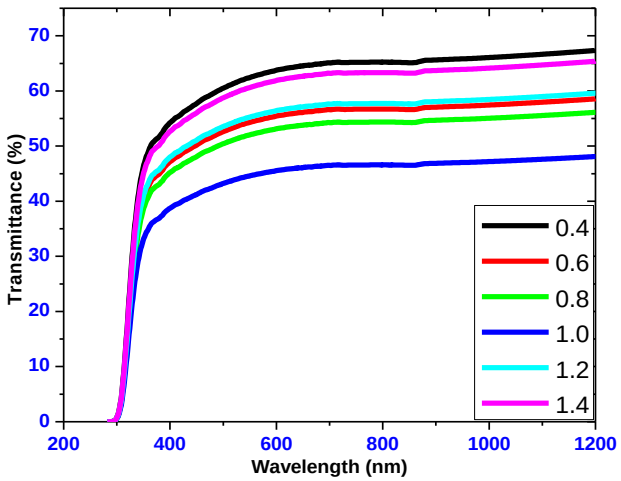

Figure 3. Transmittance spectra against wavelength for Sn_xSe_y in various ratios

A slight increase in transmittance beyond the visible range (> 750nm) was observed. This could be associated with low energy of photon making absorption to be low. The transmittance increased as the ratio of Sn:Se approached the stoichiometric values. Transmittance decreased with increase in selenium ratios and after attaining a ratio of 1:1 it again increased. This was attributed to the change in films band gaps. The film with a ratio of 1:1 had the highest absorption which was a good material for p type semiconductor.

3.1.2. Reflectance Spectra for Tin Selenide (Sn_xSe_y) Thin Films

Spectra of optical reflectance for tin selenide is shown in Figure 4. The graph shows that the reflectance within the visible region was less than 10% for all the samples. This indicates that the films had high absorption and thus can make them good absorber layer for photovoltaics.

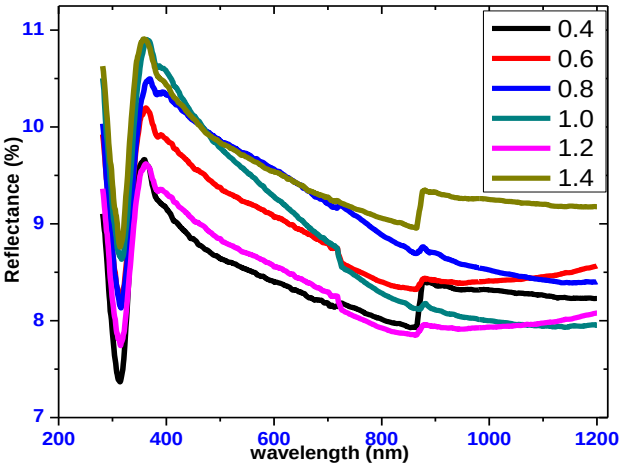

Figure 4. Optical reflectance spectra of tin selenide in various ratios

3.1.3. Absorbance Spectra for Tin Selenide (Sn_xSe_y) Thin Films

Figure 5 shows spectra of optical absorbance of tin selenide. The absorbance decreases with increase in wavelength. At lower wavelengths the photons has high energy compared to the band gap energy hence a lot of it is absorbed. SnSe ratio of 1:1 has the highest absorbance in VIS region.

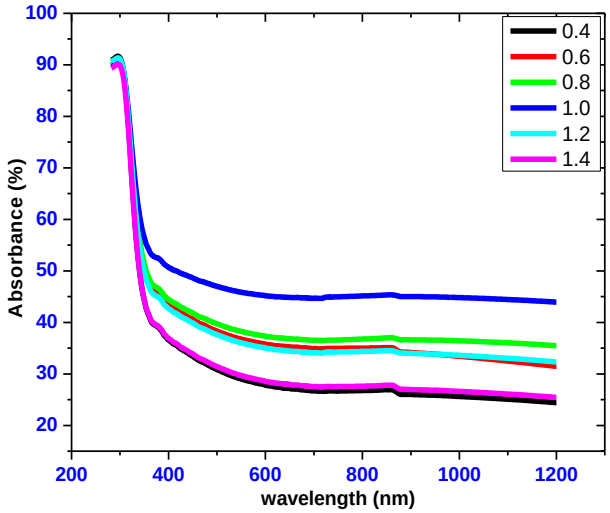

Figure 5. Optical absorbance spectra of tin selenide in various ratios

3.1.4. Absorption Coefficient for Tin Selenide (Sn_xSe_y) Thin Films

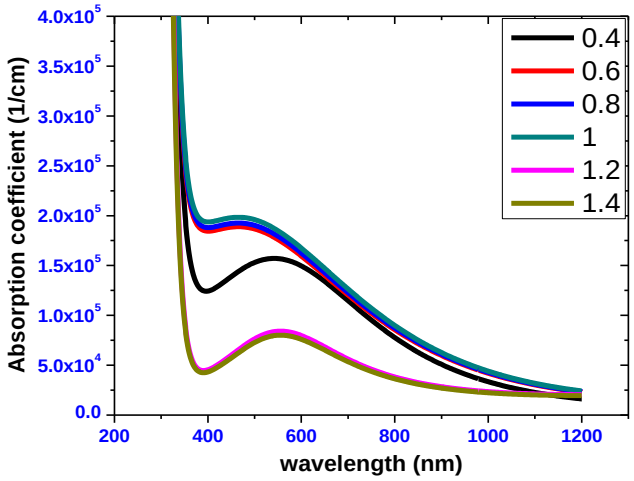

Figure 6. The absorption coefficient for different tin selenide ratios versus wavelength

Absorption coefficients at different ratios for tin selenide with varying wavelength from 280 nm to 1200 nm is shown on figure 6. From the curves, at lower wavelengths high absorption coefficients were obtained for the different tin-selenium samples. For all the samples the average absorption coefficient within the visible range (400-780) nm increases with increasing tin-selenium ratio up to a ratio 1:1 and then decreases. The Sn:Se gave an average absorption coefficient > 10^5 cm^{-1} thus making it a dependable material for casting a good absorber layer for solar cells [20]. Electrons in the valence band absorbs the photons hence excited into the conduction band.

3.1.5. Extinction Coefficient for Tin Selenide (Sn_xSe_y) Thin Films

Figure 7 shows the extinction coefficient against wavelength. As the tin selenide ratios increases, extinction coefficient increases. The film of ratio 1:1 recorded the highest extinction coefficient, this implies that its rate of absorption is good.

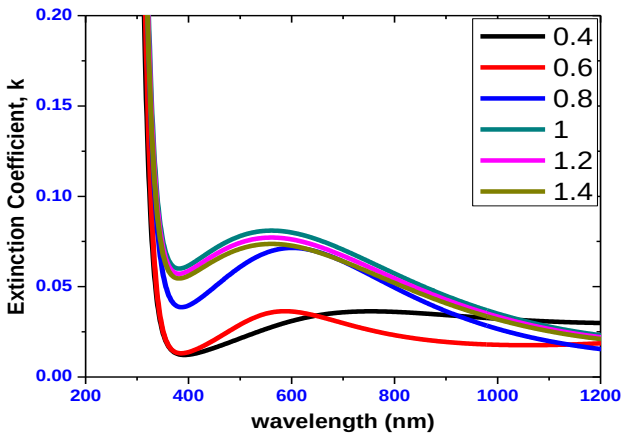

Figure 7. Extinction coefficient against wavelength of SnSe thin films for various tin selenide ratios

3.1.6. Refractive Index for Tin Selenide (Sn_xSe_y) Thin Films

The variation of refractive index of Sn_xSe_y thin films against wavelengths is shown on figure 8. As wavelength increases, it is observed that the refractive index decreases. Important to note is that a ratio of SnSe as the highest refractive index implying that it is a good absorber material this is because the radiation takes a longer time through the film using.

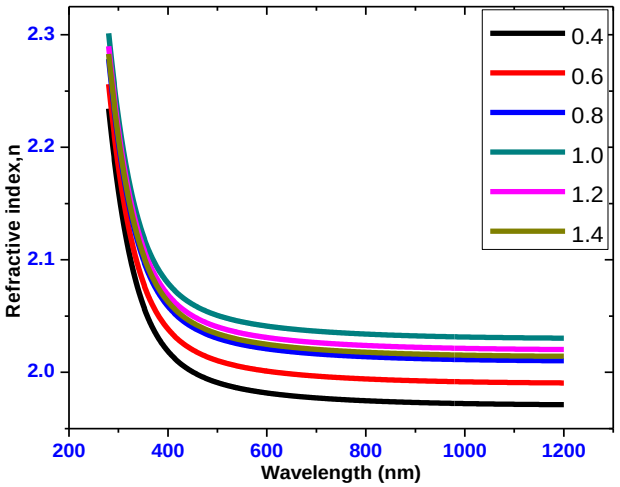

Figure 8. Refractive index versus wavelength of SnSe of varying ratios

$$n = \frac{c}{v}. \quad (8)$$

where c is the speed of light c = 2.998 × 10^8 ms^{-1}, n is the refractive index and v the speed of light in a medium.

3.1.7. Averages of Transmittance, Absorbance and Reflectance in VIS Region of Sn_xSe_y

Figure 9 shows how averages of transmittance, absorbance and reflectance of SnSe thin films varied with Sn_xSe_y ratios within visible region. It is clearly seen a sample of ratio1:1 has the highest absorbance. The average transmittance for all the samples in VIS region was below 65%, reflectance for all the samples was below 10% and absorbance below 50%. A sample of SnSe of ratio 1:1 has the highest absorbance making it a good absorber layer. Optimization of SnSe using average absorbance (%) in VIS region against sample ratios.

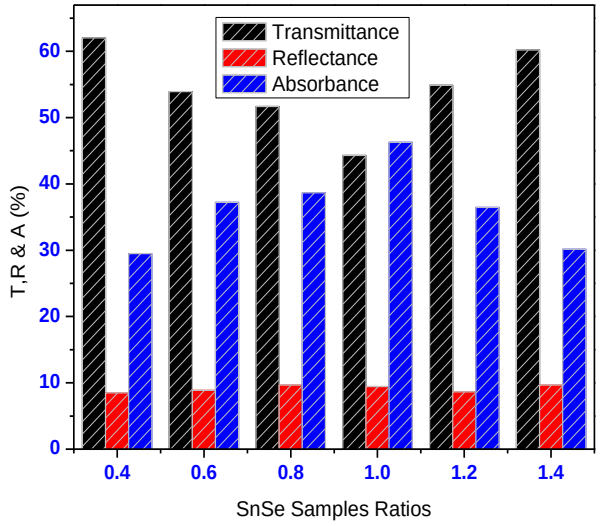

Figure 9. Shows how averages of transmittance, reflectance and absorbance of SnSe thin films varied with ratios in visible region

3.1.8. Optical Band Gap Energies for Tin Selenide (Sn_xSe_y) Thin Films

A graph of $(E\alpha)^2$ against energy drawn using data from Scout 98 programme was used to calculate the band gap energy. From the optical absorbance vs. wavelength data was obtained and using equation

$$(\alpha h\nu)^2 = A(h\nu - E_g) \quad (9)$$

mathematical treatment was done to derive the transition type and the band-gap energy. The SnSe samples optical band gap energy rest at 1.39-2.23±0.05 eV and lowest band gap energy being found on the Sn:Se ratio of 1:1 sample. The values of band gap reported by [9] for Sn_xSe_y lie between 1.18-1.85±0.05 eV and 1.18eV to 1.75eV as reported by [17].

A graph of forbidden gap energy against Sn:Se ratios is shown on figure 10. The Sn:Se thin film ratio is 1:1 had the least forbidden gap energy of 1.39±0.05 eV.

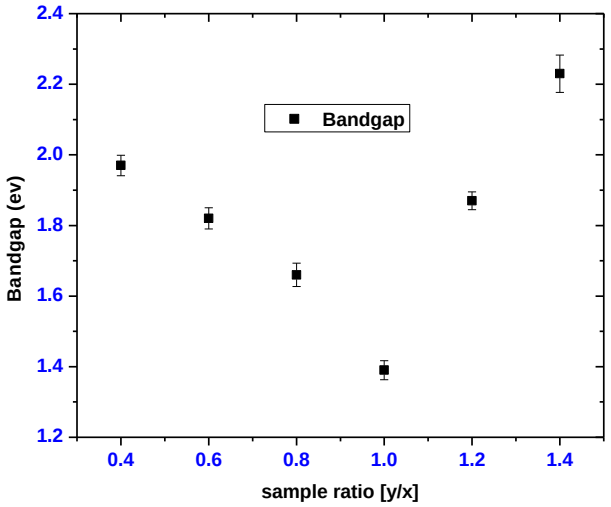

Figure 10. SnSe thin films of forbidden energy band gap varying with ratios

3.2. Nickel Doped Tin IV Oxide (SnO_2: Ni)

3.2.1. Optical Transmittance Spectra for SnO_2: Ni Thin Films

Figure 11 shows the optical transmittance for nickel doped tin IV oxide at different doping percentages. The optical transmittance of SnO_2 and Nickel doped SnO_2 was found to be above 75% in the VIS and NIR region.

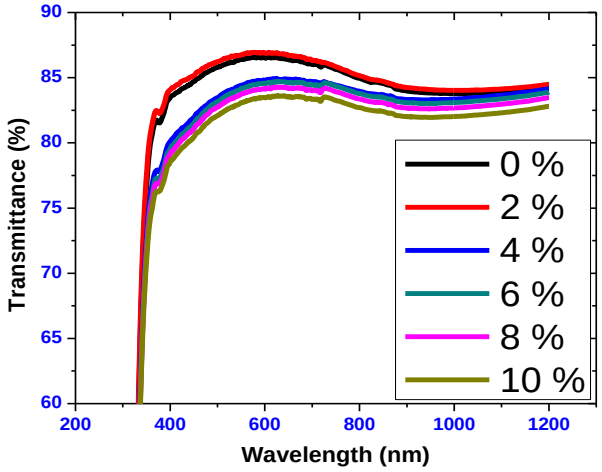

Figure 11. Graph of transmittance spectra of Tin oxide doped with thin Nickel Films

As the wavelength of illuminated photon energy increases transmittance increases briskly to maximum as verified from the spectral data. Transmittance for all the samples is highest within the visible region. Transmittance decreases for photons of wavelength beyond 750nm. This is associated with the increase in optical scattering caused by rough surface morphology. Since the photon energies are less than or too close to forbidden gap of the thin films, low optical absorption takes place resulting to higher transmittance. Unlike other samples the 2% Nickel doped sample depicted

to some extent higher transmittance. Transmittance then slightly decreases after 2% as Nickel concentrations increased. This is attributed to free charge carriers coupling to the electric field [23].

3.2.2. Optical Reflectance Spectra for SnO_2: Ni Thin Films

The plots in Figure 12, displays a spectra of reflectance. Reflectance was low and lying in the range of 8-10% in the infra-red region, ultra violet and visible range of the solar spectrum. For both doped and undoped SnO_2 the overall reflectance is fairly low. At around 850 nm a kink is observed, this is caused during the exchange of hydrogen lamp and Deuterium lamp.

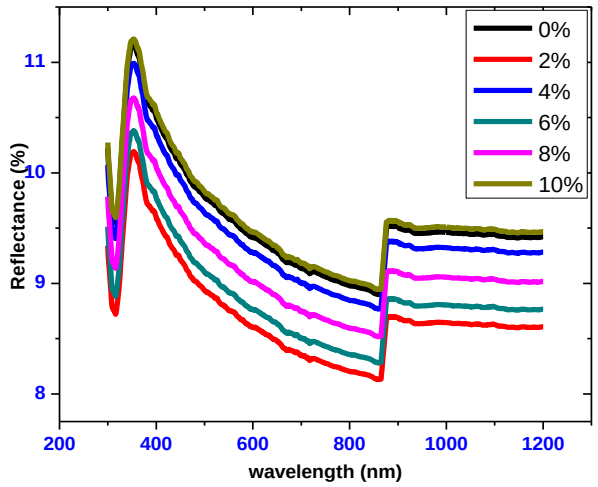

Figure 12. Optical reflectance spectra for Nickel doped Tin oxide

3.2.3. Refractive Index for Nickel Doped Tin Oxide

Refractive indices decreased against wavelength from 280-325 nm as shown in Figure 13. There were no meaningful vicissitudes of refractive indices as wavelength increased from 325-800 nm for undoped and doped Tin oxide. 2% Nickel doped tin IV oxide recorded the least refractive index. This means the photons travels through the film faster hence absorption is minimal.

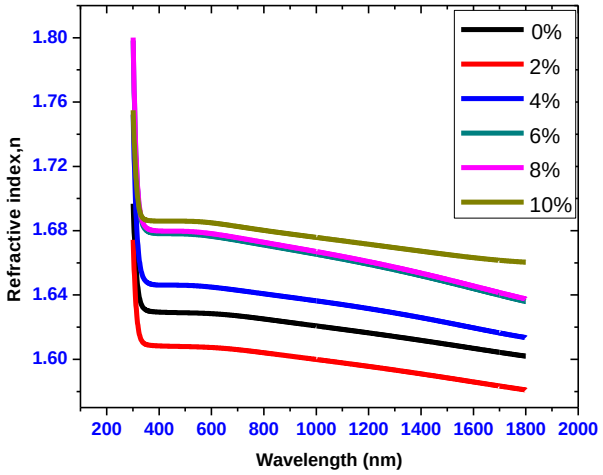

Figure 13. Refractive index versus wavelength for Nickel doped Tin oxide

3.2.4. Absorption Coefficient for Nickel Doped Tin IV oxide

Figure 14 shows absorption coefficient for SnO_2: Ni samples. The SnO_2: Ni has a low absorption coefficient at high wavelengths and a high absorption coefficient at low wavelengths. Absorption of illuminated photon is higher at lower wavelengths hence high absorption coefficient as seen in the figure. This occurs because at lower wavelength, photons have high energy compared to the band gap and therefore very well absorbed. There was an observed lowest average absorption for films with 2% Nickel doping concentration within the visible range. At high wavelengths we observe very low absorption. This is because at high wavelengths, the photons have low energy hence mainly transmitted since band gap energy is not exceeded.

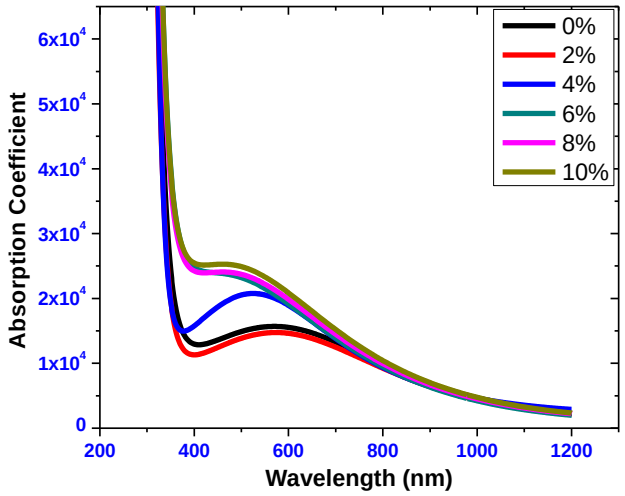

Figure 14. Absorption coefficient versus wavelength for Nickel doped Tin IV oxide

3.2.5. Extinction Coefficient for Nickel Doped Tin IV oxide

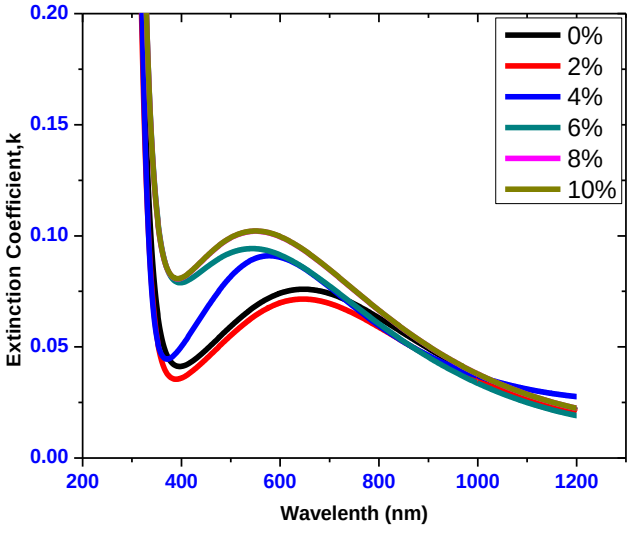

Figure 15. Extinction coefficient versus wavelength for Nickel doped Tin IV Oxide

Figure 15 shows the extinction coefficient versus wavelength. The average extinction coefficient within the visible range was below 0.2. The extinction coefficient is to a great extent increased at low wavelengths (< 350nm). This indicates that at low wavelengths, the films have high absorption. The extinction coefficient is also decreased at higher wavelength (> 750nm), this implies that the material became almost transparent at higher wavelengths. A film of 2% has the lowest extinction coefficient in the visible region.

3.2.6. Averages of Transmittance, Absorbance and Reflectance in Visible Region for Nickel Doped Tin IV Oxide

Figure 16 shows how averages of transmittance, reflectance and absorbance of Nickel doped Tin oxide thin films varied with Nickel concentration in visible region. It is clearly seen a sample of 2% Nickel has the highest Transmittance. The average transmittance in VIS region is above 80% whereas reflectance and absorbance are below 10% for the samples. This is in close range with the 1.5% Ni doped SnO_2 optimized by [4]. Therefore 2% Nickel doped SnO_2 shows properties of a good window layer for photovoltaic applications.

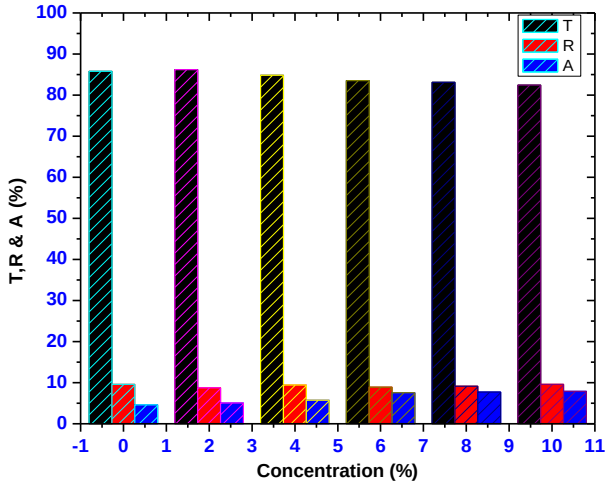

Figure 16. Shows how averages of transmittance, reflectance and absorbance of Nickel doped Tin IV oxide thin films varied with ratios in visible region

3.2.7. Optical Band Gap Energies for Nickel Doped Tin IV Oxide

The band gap energy values for Nickel doped Tin IV oxide were calculated by the scout 98 program. Using the mathematical treatment of the data the transition type and the band-gap energy can be derived from the optical absorbance against wavelength using equation 9.

Since Nickel doped Tin IV oxide is a direct allowed band gap. Figure 17 shows how to obtain the band gap using Tauc relation. When a linear graph is drawn the band gap of the sample is obtained at a point where the line cuts the energy axis.

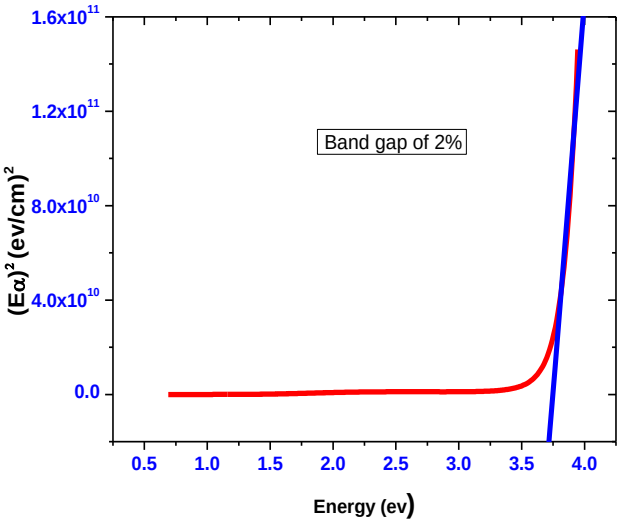

Figure 17. A graph showing how to obtain the band gap for Nickel doped Tin oxide using Tauc relation equation 9

The range of the energy band gap of Ni doped SnO_2 was between 3.65-3.75 eV. [13] Reported the energy band gap of Nickel doped Tin IV oxide values to lie between 3.70 eV and 3.76 eV. Figure 18 shows the optical band gap energy against doping concentration.

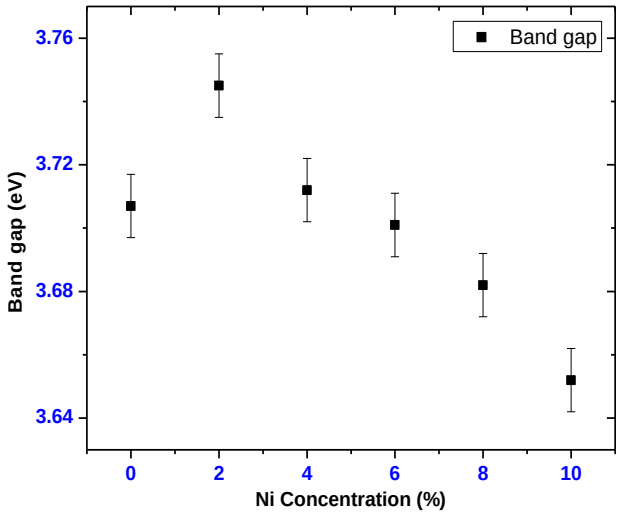

Figure 18. Graph of band gap energy with varying doping concentration

In the range of 0-2 % Ni doping, increase of band energy gap was noted. This is associated with the combined effect of Burstein-Moss effect and band gap narrowing [1]. When the conduction band edge density of states is exceeded by carrier concentration, this effect that occurs which match to degenerate doping in semiconductors. More and more donor states are wrought as the doping level concentration increases which slightly shift Fermi level in higher energy. From 2-10% Ni doping there is decrease in forbidden gap attributed to creation of new donor levels in the band gap due to the shift in the Fermi level therefore change in the band structure of the films.

3.3. Fabrication and Characterization of SnSe-SnO_2: Ni p-n Junction

Fabrication of the p-n junction solar cell with glass/SnO_2: Ni/SnSe/Al was achieved in stages. The SnO_2: Ni film which acts as a window layer, in this case n type layer was coated onto a microscope glass substrate and an absorber thin film of SnSe coated onto SnO_2: Ni on the same substrate to make a p-type layer. Fabrication was completed by deposition of Aluminium as rare contact on SnSe film to complete the solar cell as shown on figure 19.

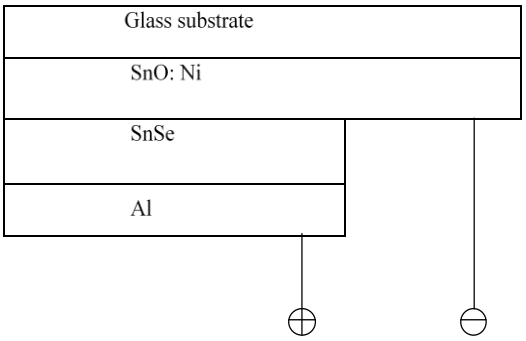

Figure 19. Fabricated SnO_2: Ni/SnSe/Al p-n junction solar cell schematic diagram

Data that was used to plot the I-V characteristics was extracted using a solar cell simulator fitted with dichroic reflector. From the I-V characteristic, short circuit current and the open circuit voltage values were obtained. When current is not flowing through the cell open circuit voltage (V_{OC}) is obtained, V (at I = 0) = V_{OC}. When the impedance is low the short circuit current (I_{SC}) is obtained which corresponds to the short circuit state and is attained when the voltage same as zero. I (at V=0) = I_{SC}. In the power quadrant, maximum current is attained known as I_{SC}, which occurs at the starting point of the forward-bias sweep. The I-V characteristic of the fabricated P-N junction solar cell is shown Figure 20.

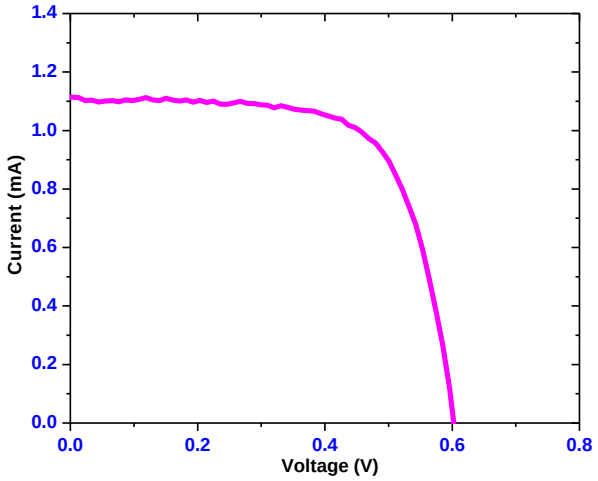

Figure 20. Simulated I-V characteristic of the fabricated SnSe-SnO_2: Ni p-n solar cell

Due to the presence of impurities that occurs during deposition process, back aluminium contact resistance and electron hole recombination, the value of short circuit current is usually low which causes the solar cell experience somewhat higher resistance to the flow of charges. The measurement of the quality of a solar cell eventually obtained by squareness of current-voltage curve is the Fill factor (FF). This is done by relating the maximum power to the theoretical power (P_T) that would be the result at short circuit current and open circuit voltage altogether.

The fabricated solar cell of an area $4cm^2$ gave the following I-V characteristic from the results owing to the solar cell simulator. The V_{OC} which is the open circuit voltage, was 0.607V and I_{SC} which is the short circuit current, was 1.118 mA/cm^2. The fill factor and conversion efficiency of the assembled solar cell were achieved using equations

$$FF = \frac{V_{max}\ I_{max}}{V_{oc}\ I_{sc}} \quad (10)$$

$$\eta = \frac{V_{oc} I_{sc} FF}{P_{in}} \times 100 \quad (11)$$

respectively. Fill factor estimate was 0.6792. Using incident power of 100W from the solar simulator's illuminated on the fabricated solar cell, the conversion efficiency (η) which is the ratio of P_{out} (the electrical power output) compared to P_{in} (the solar power input) into the solar cell was attained as 0.4609%.

4. Conclusions

The efficiency of 0.4609% was quite low in comparison to Beyond 11% efficiency: Characterization of state of the art $Cu_2ZnSn(S,Se)_4$ solar cells. Recent performance enhancement in $Cu_2ZnSn(S_{1-x}Se_x)$(CZTSSe) devices, in which indium and gallium from CIGSSe are replaced by a more abundant and lower cost Zinc and tin have efficiencies of over 11%. Evidence has shown moderate thickness of the absorber layer CZTSSe (about 200 nm thickness) and a band gaps in the range 1.08 – 1.12 eV. A Ni-AL collection grid and ~ 110 nm thick MgF_2 antireflection coating were deposited. Scanning electron Microscopy (SEM) was conducted. Scanning transmission electron microscopy (STEM) images were taken [26].

CZTSSe (Kesterite – type crystal structure) was reported in 1996 to have an efficiency of 0.66%. Subsequent optimization using both evaporation and sputtering led to performance of 6.7% in 2008. Hydrazine – based deposition process was announced with efficiency of 9.7% which further improved to 10.1% in 2011. The highest certified power conversion efficiency at the 11.1% level was reported in 2012 [26]. Further studies on SnO_2: Ni/SnSe and modern performance enhancement can lead to improvement of this efficiency.

ACKNOWLEDGEMENTS

The authors would like to thank University of Nairobi, Kenyatta University and Chuka University Physics Departments for their support.

REFERENCES

[1] Ajimsha, R.S., Das A.K., Singh, B.N., Misra,P., Kukreja, L.M. (2011). Correlation between electrical and optical properties of Cr:ZnO thin films grown by pulsed laser deposition. *Laser Materials Processing Division, Raja Ramanna Centre for Advanced Technology, India* 406: 4578-4583.

[2] Bindu, K. and Nair, P. (2004). Semiconductor tin selenide thin films prepared by heating Se-Sn. *Journal of Semiconductor Science and Technology* 19: 1348-1353.

[3] Brennan, K.F. (1999). The Physics of Semiconductors with applications to Optoelectronic Devices. *Cambridge University Press, London.*

[4] Chuah, L. S., Yaacob, M. S., Hassan Z. (2012). Low temperature synthesis of Ni-doped SnO2 thin films by spin coating route. *Physics Section, School of Distance Education, Universiti Sains Malaysia,* Vol. 6, No. 1-2:p. 149 – 153.

[5] Fahrenbruch, A. L. and Bube, R. H. (1983). Fundamentals of Solar cells. *New York Academic Press.*

[6] Jeewan, S. G., Singh, A., Thakur, G.S., Saini, N., Goyal, and Tripathi, S. K. (2005). Preparation and characterization of SnSe nanocrystalline thin flms. *Journal of Optoelectronics and advanced Materials;* 7, 2085.

[7] Jorge S. N. R., Aaron S., Juarez D., Martinez-Escobar, Manoj R. (2015). Structural and electrical characterization of snse and snse2 thin films deposited by Ultrasonic spray pyrolysis. 1: 34.

[8] Korotcenkov, G., Brinzari, V., Boris, I. (2008). (Cu, Fe, Co, or Ni)-doped tin dioxide films deposited by spray pyrolysis: doping influence on film morphology. 43:2761–2770.

[9] Kumar, N. (2010). Influence of the substrate temperature on the structural, optical and electrical properties of tin selenide thin films deposited by thermal evaporation method. *Crystal Research Technology,* 45: 53-58.

[10] Kumar, N., Sharma, V., Parihar, U., Sachdeva1, R., Padha, N. and Panchal, C. (2011). Structure, optical and electrical characterization of tin selenide thin films deposited at room temperature using thermal evaporation method. *Nano-Electronic Physics,* 3: 117-126.

[11] Kumar, N. (2012). Effect of Film Thickness on Optical Properties of Tin Selenide Thin Films Prepared by Thermal Evaporation for Photovoltaic Applications. 2: 41-45.

[12] Kuo-Jui, H. (2010). Electron-Reflector strategy for CdTe thin-film solar cells. *PhD Thesis. Colorado State University, Department of Physics, New york.*

[13] Kuppan, M., Kaleemulla, S., Madhusudhana, R. N., Sai Krishna N., Rigana, B. M., and Shobana, M. (2014). Structural and Magnetic Properties of Ni Doped SnO_2. *Research Article*. 284237:1-5.

[14] Lindgren, T., Larsson, M. and Lindquist, S. (2002). Solar Energy Materials. *Journal of Solar Cells,* 73: 377-377.

[15] Mariappan, R., Ragavenda, M., and Gowrisankar, G., (2010). Growth and characterization of SnSe thin films prepared by spray pyrolysis technique 7: 211 -216.

[16] Mohd, A., Syafiq, Y., Zainal, T. and Wan, Y. (2011). Annealing and light effect on structural and electrical properties of thermally evaporated Cu_2SnSe_3 thin films. *Chemical Engineering and Materials Science,* 2: 103-109.

[17] Nyakundi, M.E. (2014). Characterization of snse-cdo:sn p-n junction for solar cell applications. *M.Sc. Thesis. Kenyatta University. Kenya*.

[18] Okereke, N.A. and Ekpunobi, A.J. (2012). Spectroscopic studies on lead selenide (pbse) and tin selenide (snse) thin films. *Journal of Optoelectronics and Biomedical Materials.* 3: 69-74.

[19] Pirog, R. (2005). World Oil Demand and its Effect on Oil Prices. *Congressional Research Service Report*.

[20] Porotmans, J. and Arkhipov, V. (2006). *Thin film solar cells fabrication, characterization and applications.* John Wiley and Sons. Chinchester. 1: 277-363.

[21] Ranjdar, M. and Ali, B. (2006). Optical Properties of Thin Film. Ministry of Higher Education Sulaimani University College of Science Physics Department, Iraq.

[22] Sharma, J., Singh, G., Thakur, A., Saini, G., Goyal, N. and Tripathi, K. (2007). Preparation and Characterization of SnSe nanocrystalline thin films. *Journal of Optoelectronics and Advanced Materials* 7: 2085-2094.

[23] Shishiyanu, S. T., Shishiyanu, T. S. Lupan, O. I. (2004). Sensing characteristics of tin- doped ZnO thin films as NO_2 gas sensor. *Department of Microelectronics and Semiconductor Devices, Technical University of Moldova* B107 (2005): 379-386.

[24] Suhail, M. H., Abdullah, M. M. and Abbas, S. L. (2012). Structural, Electrical and Photoluminescence properties of In_2O_3 – Doped SnO_2. *Journal of Chemical, Biological and Physical science* 2: 1963-1973.

[25] Theiss, W. in: W. Theiss (Ed.), 2001. Scout Thin Film Analysis Software Handbook, Hard and Software, Aachen, Germany, *www.mtheiss.com*, pp: 54-57.

[26] Todorov, T. K., Jiang, T., Santanu B., Oki G., Tayfun G., Yu, Z., and David B. M. (2013). Beyond 11% Efficiency: Characteristics of State-of-the-Art $Cu_2ZnSn(S,Se)_4$ Solar Cells. *Adv. Energy Mater.* 3, 34–38.

[27] Toshiyuki, Y., Jiro, M. and Akira, Y. (1991). Thin films of CuInSe2 prepared by RF sputtering from various compositional powder targets: *Solar Energy materials and solar cells* 27: 25-35.

[28] Vadivel, K., Arivazhagan, V. and Rajesh, S. (2011). Room Temperature Ferromagnetism of Ni Implanted SnO2 Nanopowders. *International journal of applied engineering research.* 1:4.

[29] Yadav, A. A., Masumdar, E. U., Moholkar, A. V., Rajpure, K. Y. and Bhosale, C. H. (2008). Gas Sensing of Fluorine Doped Tin Oxide Thin Films Prepared by Spray Pyrolysis. *Journal of Sensors & Transducers* 92: 55-60.

[30] Zainal, Z., Nagalingam, S., Kassim, A., Hussein, M. and Yunus, W. (2003). Tin Selenide thin films prepared through combination of chemical precipitation and vacuum evaporation technique. *Material Science*, 21: 225-233.